

Heat production and heat flow in the mantle lithosphere, Slave craton, Canada

James K. Russell*, G.M. Dipple, M.G. Kopylova

*Department of Earth and Ocean Sciences, The University of
British Columbia, Research Institute for Geochemical Dynamics,
Department of Earth & Ocean Sciences, University of British Columbia, Canada*

Received 17 April 2000; received in revised form 23 October 2000; accepted 23 October 2000

Abstract

Thermobarometric data for mantle xenoliths from a kimberlite pipe in the NWT, Canada are used to constrain the thermal properties of the lithospheric mantle underlying the Slave craton. We derive an analytical expression for a steady-state conductive mantle geotherm that is independent of the geometry and thermal properties of the crust. The model has an upper boundary coincident with the MOHO at a depth Z_m and has temperature T_m and heat flow q_m . The mantle is assumed to have constant radiogenic heat production (A) and we allow for a temperature-dependent thermal conductivity [$K(T) = Ko(1 + B(T - T_m))$]. Inverting the thermobarometric data through the model geotherm gives limiting values for mantle heat production (A) and bounds on the temperature dependence of K (e.g. B) that are consistent with the mantle P – T array. We characterize the Slave lithospheric mantle in terms of three critical parameters q_m (mW m^{-2}), A ($\mu\text{W m}^{-3}$), T_m ($^{\circ}\text{C}$). The optimal solution has values [15.1, 0.012, 455]. This characterization of thermal state of the Slave mantle is based mainly on petrological data and is not biased by assumptions about crustal thermal properties. Our analysis shows that a substantial range of parameter values can be used to describe the data accurately and the two bounding solutions are [24.2, 0.088, 296] and [12.3, 0, 534], respectively. However, model parameters are strongly correlated and this precludes the arbitrary selection of values of [q_m , A , T_m] from these ranges. © 2001 Elsevier Science B.V. All rights reserved.

Keywords: Mantle; Craton; Radiogenic heat production; P – T array; Model; Inversion

1. Introduction

Many of the fundamental chemical and physical characteristics of cratonic mantle are established by direct study of mantle xenoliths hosted by kimberlite magmas. Kimberlite magmas derive from depths that allow for sampling of the entire mantle lithosphere and the uppermost asthenosphere (>200 km; Bailey, 1980; Nixon et al., 1981; Boyd, 1987). They also have high ascent rates that help preserve tex-

tures, mineral assemblages and mineral compositions indicative of deep mantle conditions. Such studies have shown the lithological diversity of cratonic mantle, in general and have established the thermal state and stratigraphy of lithospheric mantle beneath most cratons (e.g. Harte and Hawkesworth, 1989; O'Reilly and Griffin, 1996; Lee and Rudnick, 1999; Boyd et al., 1997; Kopylova et al., 1999a, b; Kopylova and Russell, 2000).

Not all aspects of cratonic mantle can be addressed by direct study of mantle xenoliths. The nature of radiogenic heat production (HP) within the mantle lithosphere is, generally, poorly constrained (e.g. Rudnik

* Corresponding author.

E-mail address: russell@perseus.geology.ubc.ca (J.K. Russell).

et al., 1998; Russell and Kopylova, 1999) and is unlikely to be resolved by direct analysis of kimberlite-hosted xenoliths (see Rudnik et al., 1998 for review). Firstly, the two main rock types in cratonic mantle, peridotite and eclogite, have substantially different heat producing element (HPE) contents and their proportions within the mantle are essentially unknown (Schulze, 1989). Secondly, kimberlite-hosted mantle xenoliths commonly show the chemical effects of mantle metasomatism associated with the production and transport of kimberlite magma (Bailey, 1980). In general, the K, Th, U contents of the xenoliths (Table 1, Appendix A) are not necessarily representative of the original, pre-kimberlite mantle (e.g. Rudnik et al., 1998).

We have elected to use an inverse modeling approach to estimate several properties of the mantle lithosphere underlying the Slave craton (Kopylova et al., 1999a, b). Our approach is to fit an analytical expression for a steady-state, conductive mantle geotherm to P - T data from peridotite xenoliths and, thereby, constrain the values of model parameters representing mantle thermal properties. Our model geotherm describes the temperature distribution and heat flow in the mantle, but is completely decoupled from crustal considerations. Inversion of the P - T data is used to explore the temperature dependence of thermal conductivity of the mantle (e.g. Schatz and Simmons, 1972; Ganguly et al., 1995; Jaupart et al., 1998) and to provide upper and lower bounds on mantle heat production. The main attribute of our modeling is that we achieve an objective description of the thermal state of the Slave mantle that is based on petrological data and is not biased by assumptions about crustal thermal properties (e.g. Pollack and Chapman, 1977; Nyblade and Pollack, 1993; Russell and Kopylova, 1999).

2. Lithospheric mantle to the Slave craton

The Slave craton is an Archean enclave within the larger proterozoic North American craton and situated within the northwest territories of Canada (e.g. Padgham and Fyson, 1992). Our view of the mantle underlying the Slave craton is based on the petrology of mantle-derived xenoliths within kimberlite pipes (Kopylova et al., 1999a, b; Kopylova and

Russell, 2000; MacKenzie and Canil, 1999; Pearson et al., 1999), on mapping studies involving mineral chemistry (Griffin et al., 1999; Grutter et al., 1999) and from seismic (Cook et al., 1997; Bostock, 1998; Bank et al., 2000), magnetotelluric (Jones et al., 2000) and heat flow (Hyndman and Lewis, 1999) surveys. These works show the Slave mantle lithosphere to extend to depths of ~ 160 – 210 km (Kopylova et al., 1999a; Griffin et al., 1999; Jones et al., 2000) to be cool relative to the Kaapvaal lithosphere (Kopylova et al., 1999b; Russell and Kopylova, 1999; Pearson et al., 1999) and to show pronounced stratification in modal mineralogy and chemical composition (Griffin et al., 1999; Kopylova and Russell, 2000). The Slave mantle also shows strong lateral heterogeneity in both its geochemical and geophysical character. Recent teleseismic results show that, in the northern portion of the Slave, the MOHO is situated at a depth of 35.4 km (Bank et al., 2000; Fig. 1A).

The Jericho pipe is a diamondiferous, group Ia, non-micaceous kimberlite. It is situated in the north central Slave craton ~ 150 km NNW of the Lac de Gras kimberlites (Cookenboo, 1998; Kopylova et al., 1999a; Price et al., 2000). Kopylova et al. (1999a) obtained mantle P - T conditions from 37 samples of peridotite and pyroxenite (Table 1, Fig. 1). These data define two populations of xenoliths (Fig. 1A): (a) low- T peridotite representing the conductive mantle geotherm and (b) a high- T peridotite suite that records a young, thermal disturbance indicative of asthenospheric influences (e.g. Boyd, 1987; Harte and Hawkesworth, 1989; Kopylova et al., 1999a). The low- T peridotite samples ($N = 25$) are used to model the steady-state conductive geotherm (see Kopylova et al., 1999a; Russell and Kopylova, 1999 for discussion).

The P - T data define the relative vertical distributions of peridotitic and pyroxenitic rock types, thereby, providing a stratigraphy for the Slave lithosphere (Fig. 1B; after Kopylova et al., 1999b). The relative distributions of eclogite (Fig. 1C) are inferred from the intersections of the equilibrium temperatures for eclogite (Ellis and Green, 1979) and the P - T array defined by peridotite samples (Fig. 1A; after Kopylova et al., 1999b). Eclogite appears to be widespread throughout the Slave mantle lithosphere, but is particularly abundant between 100 and 160 km.

Table 1

Compilation of data on mantle xenoliths from Jericho kimberlite pipe used to model mantle geotherm, including geothermobarometry results based on Brey and Kohler (1990) and values of heat production based on chemical compositions of xenoliths

No.	T (°C)	P (kb)	K (%)	U (ppm)	Th (ppm)	HP ^a ($\mu\text{W m}^{-3}$)
Coarse spinel peridotite (low- T)						
$N = 3^b$	–	–	0.08–0.17	0.9–1.8	0.2–0.3	0.15–0.27
Coarse spinel + garnet peridotite (low- T)						
36617	932	49.4				
25-4	975	47.7				
21-1	811	30.8	0.12	0.9	0.1	0.1253
36770	809	32.8	0.12	1.3	0.2	0.1922
22-5	951	42.9				
41-4	648	25.2				
22-1	690	26.7				
22-4	833	36				
40-7	967	44.8				
26-11	944	42.7				
26-3	833	35.9				
Coarse garnet peridotite (low- T)						
14-77	912	41.6				
25-9	842	36.6				
36618	921	42.2				
14-107	1068	51.6				
40-11	1104	52.1				
21-6	1190	62.2				
26-3	833	35.9				
36648	918	41				
21-4	1097	55.2				
Porphyroclastic garnet peridotite (high- T)						
21-2	1335	57.7				
22-7	1187	53.4				
23-5	1262	59.2	0.11	1.4	0.3	0.2308
40-9 ^c	1297	56	0.07	0.9	b.d.	0.0963
41-1	1274	55.5				
40-21	1273	54.7				
40-36	1245	53.5				
36738	1282	56.4				
14-78	1300	59				
21-3	1088	51.2	0.36	3.7	0.3	0.4614
40-38	1286	49.5				
40-5	1300	54.4				
Pyroxenite & megacrystal assemblages (high- T)						
26-12	1246	65.1				
36778	1214	62.9	0.17	0.8	0.3	0.1862
14-124	1230	64.2				
14-105	1205	60				
41-3	1281	60				

^a Radiogenic heat production is computed for a mean density of 3300 kg m^{-3} .

^b Equilibrium P – T conditions could not be estimated for these three samples of spinel peridotite.

^c Sample was analyzed in duplicate.

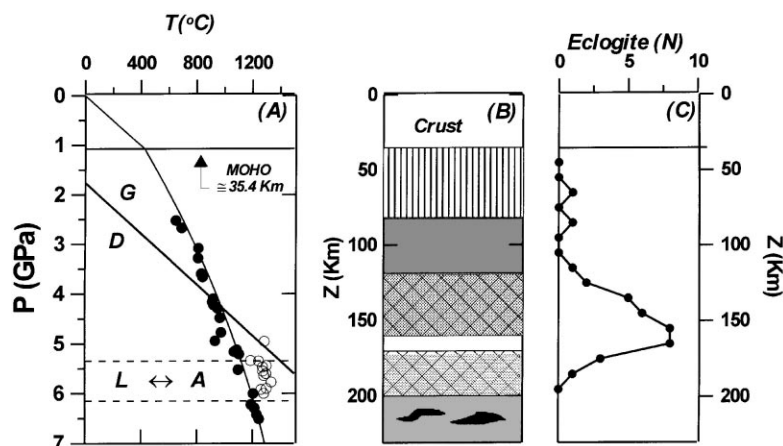


Fig. 1. Summary of Slave mantle properties based on studies of mantle xenoliths from Jericho kimberlite pipe (see Kopylova, et al., 1999a, b). (A) P - T array for low- T (solid) and high- T (open) peridotite xenoliths and graphite (G)-diamond (D) stability fields. High- T peridotite defines the transition from lithosphere to asthenosphere (L-A). (B) Stratigraphy of Slave mantle, including: spinel peridotite (vertical bars), spinel + garnet peridotite (solid grey), garnet peridotite (white) and porphyroclastic peridotite (light grey). Cross hatch pattern denotes regions of overlap, solid black represents pyroxenitic and megacrystal assemblages. (C) Apparent depths of eclogite xenoliths within Slave lithosphere.

3. Heat production considerations

Values of radiogenic heat production within cratonic mantle lithosphere vary between 0 and $0.04 \mu\text{W m}^{-3}$ and are largely based on the expected concentrations of U, Th and K in depleted peridotite (Fig. 2; Cer-

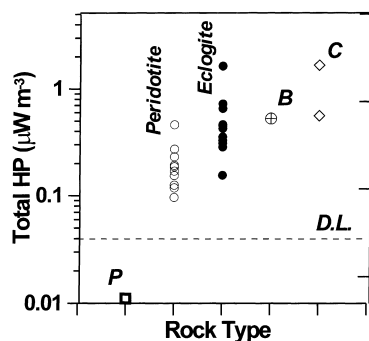


Fig. 2. Heat producing properties of xenoliths from Slave mantle (from measured K, U and Th contents; Table 1 and Appendix A) are compared to average values for continental crust (C), basalt (B) and peridotite (P) (Cermak et al., 1982; Carmichael, 1984; Rudnik et al., 1998). Dashed line marks limits on calculated HP due to analytical detection limits (Appendix A).

mak et al., 1982; Carmichael, 1984; Rudnik et al., 1998). The concentrations of U, Th and K implied by these values of radiogenic heat production are essentially at detection levels for many analytical methods (cf. Fig. 2; Appendix A). Even at these low concentrations of HPE, cratonic mantle lithosphere contributes enough radiogenic heat to impact global heat flow budgets because the volume of material is large (e.g. >150 km thick). Furthermore, accurate representation of cratonic mantle heat production is important to the interpretation of both surface and mantle heat flow. For example, HP values for mantle lithosphere of 0.02 – $0.04 \mu\text{W m}^{-3}$ over a thickness of 150 km contribute 3 – 6 mW m^{-2} to the reduced (heat flow at the MOHO) or surface heat flow regime.

Estimating heat production in cratonic mantle is complicated by the presence of diverse rock types, including eclogite (Fig. 1C). Eclogite is common in cratonic mantle lithosphere (e.g. Schulze, 1989) and in the Jericho kimberlite, it comprises 75% of the mantle-derived xenoliths (Kopylova et al., 1999b). Many eclogite xenoliths probably derive from oceanic (basaltic) crust (Helmstaedt and Schulze, 1989; Kopylova et al., 1999b) and thus, can have

HP values 20 times, or more, in excess of depleted mantle (e.g. $0.02\text{--}0.04 \mu\text{W m}^{-3}$; see Rudnik et al., 1998). If the mantle lithosphere contained 10 vol.% of eclogite, this would cause a two- to three-fold increase in mantle heat production. For a 150 km thick mantle lithosphere, this is an additional $5\text{--}11 \text{ mW m}^{-2}$ contribution to reduced or surface heat flow.

Even where the stratigraphy of the mantle is well-established (e.g. north central Slave; Fig. 1B), it is difficult to compute an accurate weighted value for mantle heat production. This is because, within kimberlite, the proportion of eclogite to peridotite xenoliths is heavily biased towards eclogite (Schulze, 1989) and does not represent mantle abundance. Schulze (1989) estimated mantle eclogite abundance to be 3–15% for several kimberlite pipes, even though eclogite comprised up to 80% of the xenolith populations.

Lastly, almost all cratonic mantle xenoliths sampled by kimberlite show effects of infiltration by metasomatic fluids enriched in K, U and Th. These fluids must predate passage of the kimberlite but are young, relative to the stabilization of the lithosphere (Bailey, 1980; Rudnik et al., 1998). Consequently, concentrations of HPE in peridotite and eclogite xenoliths are not indicative of the concentrations in primary,

undisturbed mantle and cannot be used to compute values of heat production for the lithospheric mantle. Xenoliths from Jericho attest to infiltration of metasomatic fluids in two ways. X-ray maps for K, Na, U and Th show these elements to be concentrated along grain boundaries of primary minerals and in secondary hydrous phases. Secondly, both peridotitic and eclogitic samples have high HPE contents (Table 1 and Appendix A). Calculated HP values for peridotite range from 0.1 to $0.46 \mu\text{W m}^{-3}$ and are substantially higher than found in conventional depleted mantle (Fig. 2). HP values for eclogite xenoliths range from 0.16 to $1.69 \mu\text{W m}^{-3}$; some samples have values equivalent to average continental crust (Fig. 2).

4. Analytical expression for mantle geotherm

We begin by solving the one-dimensional boundary value problem for steady-state conductive heat flow in the lithospheric mantle. Our solution departs from other models (e.g. Pollack and Chapman, 1977; Nyblade and Pollack, 1993; Rudnik et al., 1998; Russell and Kopylova, 1999) in that it decouples mantle heat flow from the structure and composition of the crust.

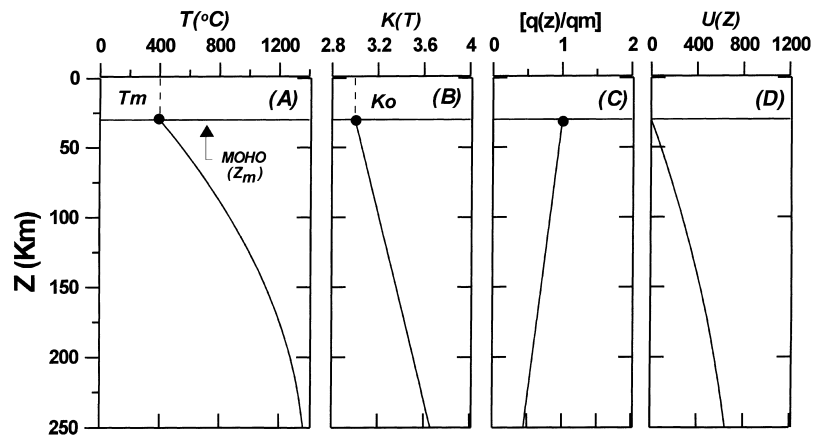


Fig. 3. Model for steady-state conductive mantle geotherm, showing: (A) geometry of model including an upper boundary (MOHO) positioned at depth Z_m and having temperature T_m , and heat flow q_m . (B) Thermal conductivity is allowed to vary linearly with temperature and has a prescribed value of K_0 at the MOHO. (C) Schematic distribution of ratio of mantle heat flow $q(z)$ to q_m for a lithosphere with radiogenic heat sources (A) and variable $K(T)$. (D) Schematic distribution of variable U representing transformed temperature (see text).

The model has an upper boundary (Fig. 3A) defined by the MOHO situated at a depth Z_m and characterized by temperature T_m and heat flow q_m . Our results are based on a value of 35 km for Z_m derived from Bank et al. (2000) for the northern Slave craton. The mantle lithosphere is assumed to have a constant and uniform value for radiogenic heat production (A). Furthermore, we allow for thermal conductivity (K) to vary with temperature (Fig. 3B). Consideration of a temperature-dependent thermal conductivity creates the non-linear boundary value problem.

$$\nabla[K(T)\nabla T] = -A \quad (1)$$

which is solved via the following boundary conditions:

$$T = T_m \quad \text{for } z = Z_m \quad (2a)$$

$$K(T) \frac{\partial T}{\partial z} = q_m \quad \text{for } z = Z_m \quad (2b)$$

The Kirchoff transformation (cf. Ozisik, 1993) is used to move K outside of the differential operator. This transformation employs the variable

$$U = \int_{T_0}^T \frac{K(T')}{Ko} dT' \quad (3)$$

where Ko is a known value of mantle thermal conductivity at a specified temperature T_0 . Eq. (3) is used to transform the boundary value problem Eq. (1), (2a) and (2b) to a new problem in $U(z)$. Using the chain rule to expand ∇T in Eq. (1), we obtain

$$\frac{\partial T}{\partial z} = \frac{\partial U}{\partial z} \frac{\partial T}{\partial U} \quad (4)$$

and using Eq. (3), we substitute the relationship

$$\frac{\partial U}{\partial T} = \frac{K(T)}{Ko} \quad (5)$$

into the expanded form of Eq. (1) to obtain the new linear differential equation in $U(z)$

$$\nabla^2 U = -\frac{A}{Ko} \quad (6)$$

This boundary value problem is valid for any form of $K(T)$ (e.g. Cermak et al., 1982; Ganguly et al., 1995; Jaupart et al., 1998). However, the attendant boundary conditions are dictated by the form of the temperature dependence of $K(T)$.

The total thermal diffusivity of mantle minerals is a composite of lattice (or phonon) versus radiative thermal diffusivities (e.g. Katsura, 1995). Experimental data show that lattice thermal diffusivity decreases with increasing temperature, whereas radiative thermal diffusivity increases with temperature. This produces non-linear variations in total thermal diffusivity with temperature (e.g. Schatz and Simmons, 1972; Katsura, 1995). Mantle thermal properties are complicated further by the effects of pressure; Katsura (1995) showed that the thermal diffusivity of olivine has a positive pressure dependence at lower temperatures but may have a negative pressure dependence at high temperature. Furthermore, the functional form of $K(T)$ developed for individual minerals (e.g. olivine) may not be applicable to the mantle lithosphere because the values of K are probably more strongly controlled by variations in rock type and texture.

We have adopted a linear model for the temperature dependence of K (Cermak et al., 1982; Carmichael, 1984; Ozisik, 1993)

$$K(T) = Ko[1 + B(T - T_0)] \quad (7)$$

where B is a coefficient relating Ko to thermal conductivity at higher temperatures. This choice has two main attributes. Firstly, the simple form of our equation ensures that we do not introduce non-linear behavior that is an artifact of a more complicated, but poorly constrained, constitutive equation (Ganguly et al., 1995; Jaupart et al., 1998). Secondly, experimental data on olivine show thermal conductivity (or diffusivity) to be linear at temperatures $>500^\circ\text{C}$. Therefore, the linear approximation is appropriate for most of the mantle lithosphere. In fact, Katsura (1995) suggests that ambient upper mantle has an almost constant value of thermal diffusivity ($7-8 \times 10^{-7} \text{ m}^2 \text{ s}^{-1}$). Eq. (7) requires the transformed boundary conditions

$$U = (T_m - T_0) + \frac{B}{2}(T_m - T_0)^2 \quad \text{for } z = Z_m \quad (8a)$$

$$Ko \frac{\partial U}{\partial z} = q_m \quad \text{for } z = Z_m \quad (8b)$$

The variable Ko is assigned to the base of the MOHO (Fig. 3B) which equates T_0 with T_m and reduces the boundary condition Eq. (8a) to $U = 0$ (Fig. 3D and

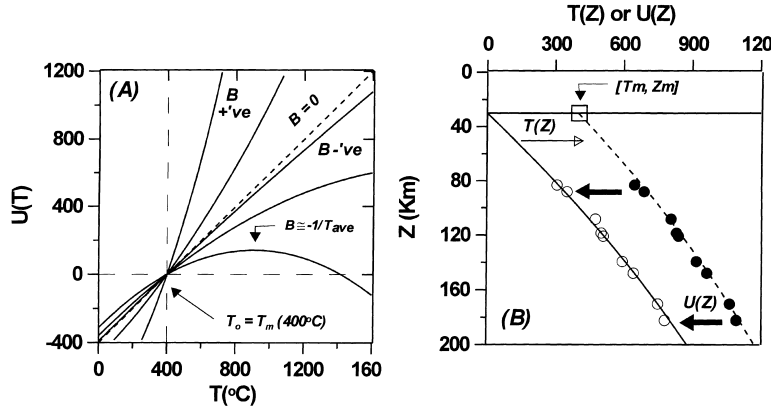


Fig. 4. (A) Variables U and T are related to B as shown graphically, at T_m they are equivalent. (B) Schematic representation of how transformed dataset U is used to solve for mantle geotherm. T - Z data are transformed into a U - Z coordinate system Eq. (10). The boundary value problem is solved in this coordinate system and then mapped back to T - Z system Eq. (11).

Fig. 4). Solution of the boundary value problem in $U(z)$ yields the following analytical expression:

$$U(z) = \frac{q_m}{Ko}(z - Z_m) - \frac{A}{2Ko}(z - Z_m)^2 \quad (9)$$

which describes the steady-state geotherm in the mantle lithosphere within U -space (Fig. 3D). The relationship between the variable U and the original values of T derives from integration of Eq. (3) after substitution of the functional form of $K(T)$ Eq. (7)

$$U(z) = [T(z) - T_m] + \frac{B}{2}[T(z) - T_m]^2 \quad (10)$$

The relationship between U and T is depicted in Fig. 4A. Conversely, the inverse transformation from $U(z)$ to $T(z)$ is

$$T(z) = \frac{(BT_m - 1) \pm \sqrt{1 + 2BU}}{B} \quad (11)$$

5. The inversion

The thermobarometric data (Table 1) provide a set of T - Z coordinates, whereas the analytical expression for the geotherm Eq. (9) is in terms of the variable $U(z)$. The variable $U(z)$ is related to $T(z)$ by Eq. (10) (Fig. 4A) and by equating Eq. (9) and (10), $U(z)$ is removed. Upon rearrangement we obtain the following

equation in $T(z)$:

$$\frac{q_m}{Ko}(z - Z_m) - \frac{A}{2Ko}(z - Z_m)^2 - \frac{B}{2}(T - T_m)^2 = (T - T_m) \quad (12)$$

This form of the equation is used to create a system of equations: one for each of the 25 samples of low- T peridotite. The equations are linear with respect to the unknown parameters A , q_m , and B and can be solved by conventional methods (e.g. Press et al., 1986). Specifically, we seek to minimize the χ^2 function

$$\chi^2 = \sum_{i=1}^n \left\langle \frac{(T_i^{\text{obs}} - f(\sum_{j=1}^m X_j))_i}{\sigma_i} \right\rangle^2 \quad (13)$$

where X_j are model parameters and the summation is over all observed temperatures (T_i^{obs}). The objective function is weighted to the mean standard uncertainty (σ_i) on temperatures arising from analytical considerations ($\pm 15^{\circ}\text{C}$). The steps to obtaining this solution are represented schematically in Fig. 4B. Conceptually, all T - Z data points are transformed to values of U - Z (Fig. 4A,B). The optimization problem Eq. (13) is solved to obtain the best model parameters; values along the model geotherm are then mapped back to T - Z space by Eq. (11) (Fig. 4B).

Table 2

Summary of variables set (e.g. K_0 , T_m and B) and model parameters (e.g. A , q_m , B and T_m) derived by fitting P – T data to steady-state conductive geotherm. All runs used a value of $Z_m = 35$ km and T_0 was assumed to equal T_m (see text)

Model	K_0 ($\text{W m}^{-1} \text{K}^{-1}$)	T_m ($^{\circ}\text{C}$)	q_m (mW m^{-2})	A (mW m^{-3})	B (K^{-1})	χ^2
q_m – A ($B = 0$)	3.2	400	18.2	0.0364	–	86.3
	3.2	450	15.4	0.0138	–	82.3
	3.2	350	21	0.059	–	97.0
	3	400	17	0.0341	–	86.3
	3.4	400	19.3	0.0386	–	86.3
q_m – B ($A = 0$)	3.2	400	17.1	–	2.85E–04	133.9
	3.2	450	14.3	–	–2.73E–05	90.9
	3.2	350	20.4	–	5.88E–04	202.0
	3	400	16.1	–	2.85E–04	133.9
	3.4	400	18.2	–	2.85E–04	133.9
q_m – T_m – A ($B = 0$)	3.2	455	15.1	0.0117	–	82.7
q_m – T_m – A	3.0 (3.4) ^a	461	13.8	0.00085	1.33E–04	73.9
q_m – T_m – A	3.0 (4.0) ^a	473	13.2	–0.0151	3.33E–04	64.7

^a Brackets enclose values of $K(T)$ at 1000 $^{\circ}\text{C}$ above model T_m .

6. Results

Below we fit Eq. (12) to a P – T array for peridotite xenoliths and thereby, constrain a set of model parameters representing properties of the Slave mantle lithosphere. In essence, we are investigating the extent to which curvature of the model geotherm is supported by the P – T array. Curvature in the steady-state mantle geotherm arises from non-zero values of mantle heat production, temperature-dependent thermal conductivity, or both. The steady-state assumption is clearly an approximation and as discussed by others (i.e. Jaupart and Mareschal, 1999), temperatures within thick mantle lithosphere are never in equilibrium with the instantaneous values of heat production. Consequently, the observed P – T array owes its geometry to a time-integrated value of heat production, rather, than being a direct measure of heat production in the mantle lithosphere at the time of kimberlite ascent. Similarly, the calculated thermal properties of the MOHO (q_m or T_m) must be accepted as estimates that reflect a time-integrated or averaged value of heat production in the lithospheric mantle.

6.1. Mantle heat production: A – q_m modeling

Our initial result assumes constant thermal conductivity ($B = 0$); inversion of the P – T array constrains

mantle heat production (A) and heat flow at the MOHO (q_m). The solutions (Table 2) are shown graphically (Fig. 5A) as ellipse-shaped regions representing 95% confidence limits on the model parameters (e.g. q_m versus A). The shaded ellipse indicates the preferred solution and is for a fixed T_m of 400 $^{\circ}\text{C}$ and an intermediate value of K_0 (3.2 $\text{W m}^{-1} \text{K}^{-1}$). The optimal solution is $q_m = 18.2 \text{ mW m}^{-2}$ and $A = 0.036 \mu\text{W m}^{-3}$ and there is strong positive correlation between model parameters. The confidence envelope has 2σ limiting values for q_m and A of 16.2–20.1 mW m^{-2} and 0.009–0.063 $\mu\text{W m}^{-3}$, respectively. These are maximum estimates of A , because all curvature in the geotherm is assigned to mantle heat production (e.g. $B = 0$).

The problem is also solved for different values of T_m (350–450 $^{\circ}\text{C}$) and K_0 (3.0–3.4 $\text{W m}^{-1} \text{K}^{-1}$) (Table 2). At lower values of T_m (Fig. 5A) the solution moves to higher values of q_m and A . Lower T_m implies a larger temperature gradient between the MOHO and the peridotitic mantle and thus, a higher heat flux. The increase in mantle-derived heat flow requires support from higher radiogenic heat production. Conversely, higher values of T_m imply less heat flow at the MOHO and require lower A . At values of $T_m > 450^{\circ}\text{C}$, the solution encloses values of $A < 0$ (Fig. 5A), implying zero heat production in the mantle. This marks the high temperature limit for T_m .

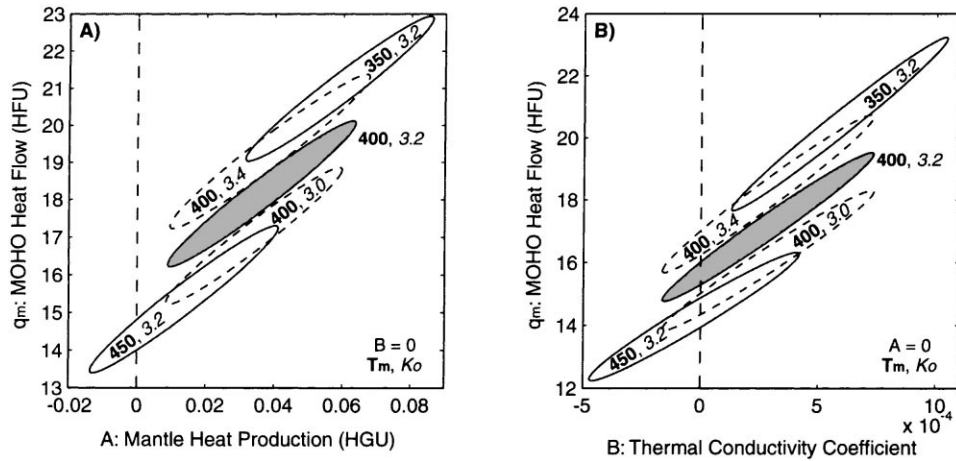


Fig. 5. Model solutions are shown as 95% confidence limits in parameter space (A) optimum solution for constant K ($B = 0$) is shown as shaded ellipse in q_m vs. A diagram (B) optimum solution (shaded ellipse) for zero heat production is shown as q_m vs. B . The effects of the variables T_m and K_o on these solutions are shown as unshaded solid and dashed ellipses, respectively, and are labeled by the changed property (see text for discussion).

Varying K_o has little impact on the solution (Fig. 5A; dashed ellipses). In fact, the optimum range of values for A change by less than 1%. Changing the values of K_o simply scales the model values of q_m by a constant factor (e.g. Jaupart et al., 1998). In summary the total range of allowed q_m is from 13.5 to 23 mW m^{-2} . Heat production is less than $0.088 \mu\text{W m}^{-3}$. In general, all solutions require a positive value for A , except at values of $T_m > 450^\circ\text{C}$ or greater; these values of T_m require, at best, zero heat production in the lithosphere and, at worse, a mantle heat sink.

The implications for model mantle geotherms are summarized graphically in Fig. 6A,B. Coordinate pairs [q_m , T_m] on the confidence limits to the preferred solution (Fig. 5A; shaded ellipse) are used to compute a family of model geotherms Eq. (9), (10) and (11) and are plotted against the original data array. We have done this in U - Z and T - Z coordinate space (Fig. 6). For this particular problem, where $B = 0$, the only difference between U and T is the constant T_m Eq. (10) and therefore, the patterns for the two families of geotherms (Fig. 6A versus B) are equivalent.

The model geotherms describe the original P - T array very well. Most importantly, the shaded fields

in Fig. 6A,B accurately portray the distribution of geotherms that are consistent with the 95% confidence limits on the model parameters q_m and A (Fig. 5A). The distribution and quality of the data (Table 1) determine the bounds on q_m and A (Fig. 5A). Fig. 6A,B is simply the mapping of those bounds into P - T space as a set of geotherms that is entirely consistent with the original P - T array. This analysis clearly demonstrates that, for example, the data are permissive of high values of heat production (e.g. $>0.06 \mu\text{W m}^{-3}$; Fig. 5A) but would require correspondingly high values of reduced heat flow (e.g. 20 mW m^{-2}).

6.2. Temperature-dependent thermal conductivity: B - q_m modeling

Our other limiting case considers no heat production ($A = 0$) in the mantle lithosphere; curvature of the P - T array is attributed to a temperature-dependent K (e.g. $B \neq 0$). For $T_m = 400^\circ\text{C}$ and $K_o = 3.2 \text{ W m}^{-1} \text{ K}^{-1}$ (Fig. 5B, shaded ellipse), the optimal solution is $q_m = 17.1 \text{ mW m}^{-2}$ and $B = 2.85\text{E}-4 \text{ K}^{-1}$. The value of B implies a 21% increase in thermal conductivity from the MOHO to the base of the lithosphere ($K \approx 3.9$). The solutions show a strong correlation

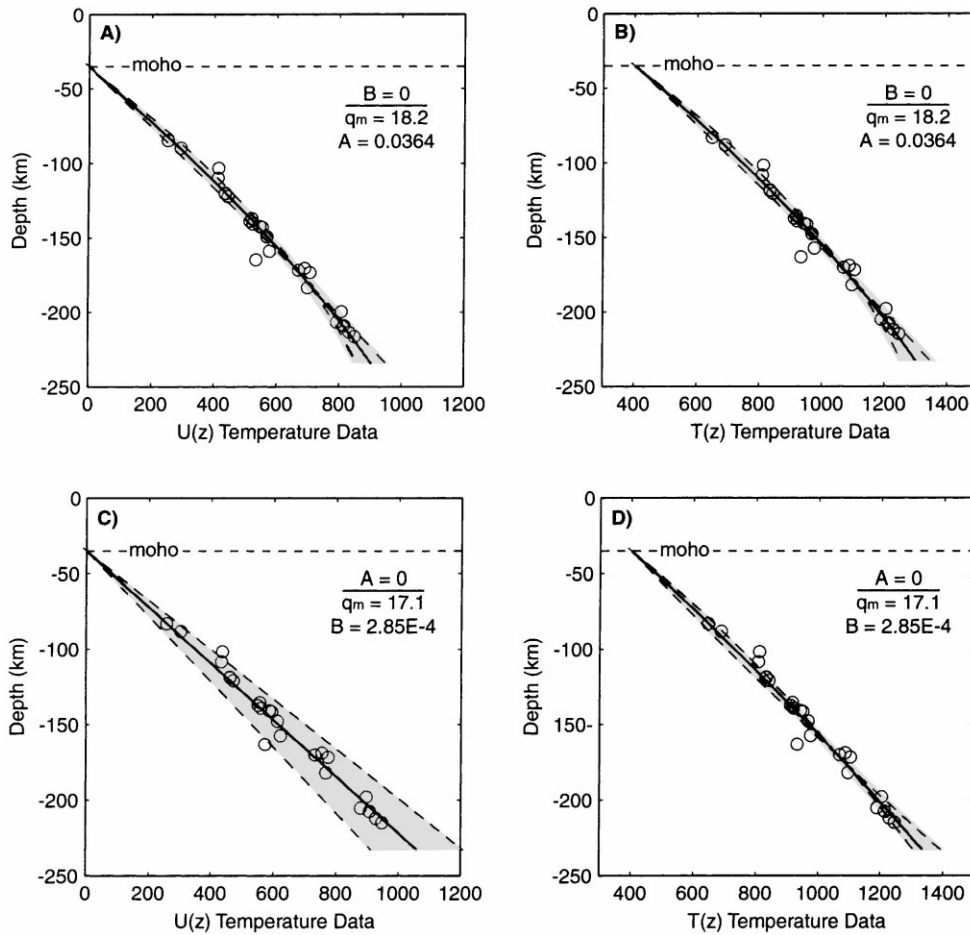


Fig. 6. Model geotherms compared to P - T data array in U - Z and T - Z coordinate space. Shading shows set of geotherms generated from coordinates on the confidence ellipses (Fig. 5). Dashed lines are geotherms from the two ends of the ellipses and do not necessarily form the boundaries to the shaded regions. Solid line is optimal solution, (A, B) field of geotherms for the q_m - A parameter model (cf. Fig. 5A) (C, D) arrays calculated for the q_m - B parameter model.

between the parameters q_m and B and the 2σ limiting values for q_m and B are 14.8 – 19.5 mW m^{-2} and $-1.63\text{E}-4$ – $7.34\text{E}-4 \text{ K}^{-1}$, respectively.

The effects of varying T_m and K_0 (Table 2) are explored in Fig. 5B. Lower values of T_m generate solutions with higher values of q_m and B . As discussed previously, the higher values of q_m are consistent with the larger temperature gradients between the MOHO and the deep mantle. In addition, large positive values of B are required to cause a concave-down curvature in the geotherm. Changing values of K_0 has similar effects on q_m - B solutions (Fig. 5B; dashed

ellipses) to those discussed for the q_m - A results (cf. Fig. 5A).

At values of $T_m > 450^\circ\text{C}$, most solutions involve negative values of B ; positive values of B are favored by lower T_m . Negative values of B cause K to decrease with T and imply a concave-up geotherm for the mantle. We have elected to consider only solutions where $B > 0$, because most of the available data suggest that K should increase with temperature under mantle conditions (e.g. Schatz and Simmons, 1972; Katsura, 1995; Jaupart et al., 1998). Applying this restriction limits the total 2σ range of values of q_m

to 13.8 to 23.2 mW m⁻² and values of B from 0 to 1.1E-4 K⁻¹.

The family of geotherms (Fig. 6C,D; shaded area) for the confidence limits on parameters q_m and B (Fig. 5B) describe the P - T data well in both U - Z and T - Z space, but they have substantially different geometries. In U - Z space the model geotherms cover a fan-shaped region (Fig. 6C); this reflects how the variances in the variable $T(z)$ are mapped to the new variable $U(z)$

$$\sigma_U^2 = [1 + B(T - T_m)]^2 \sigma_T^2 \quad (15)$$

At the MOHO ($T = T_m$) the variance in U and T is equal but at depth (e.g. $T > 1000^\circ\text{C}$), the corresponding variance in U increases. Furthermore, the U - Z model geotherms are linear, having a slope of $q_m/K\alpha$ and are symmetrically distributed about the optimal solution. In the T - Z domain, the geotherms describe a set of cross-cutting and overlapping curves that are dependent on B Eq. (11). Positive values of B generate concave down geotherms. Negative values of B produce arrays that are concave-up.

This behavior is best exemplified by the “end-point” geotherms (Fig. 6D, dashed lines) defined by the highest and lowest pairs of parameter values (e.g. q_m - B ; Fig. 5B). In T - Z space, the geotherm with the highest coordinate pair starts with the highest slope (q_m) and shows the greatest concave-down curvature ($B > 0$). The other geotherm begins with a low slope but increases along a concave-up ($B < 0$) curve. The two curves intersect and cross-over at depth. The set of model geotherms need not be symmetrically distributed about the best-fit geotherm in T - Z space (Fig. 6D; solid line). Furthermore, the “end-point” geotherms do not necessarily enclose all of the permissible T - Z coordinates (compare shaded region to dashed lines; Fig. 6D).

6.3. Thermal properties of the Slave mantle: estimates of q_m - A - T_m

Lastly, the P - T array has been inverted for simultaneous estimates of the mantle properties q_m - A - T_m using Eq. (12) and (13) in a slightly rearranged form.

Thermal conductivity can vary with temperature but B is independently fixed at zero or set to an appropriate positive value (Table 2). Results for the case $B = 0$ provide a maximum estimate for mantle heat production (A) (Figs. 7–9; Table 2). The optimal solution has values $q_m = 15.1 \mu\text{W m}^{-2}$, $A = 0.012 \mu\text{W m}^{-3}$, $T_m = 455^\circ\text{C}$.

Confidence limits on the solution describe a three-dimensional (3-D) ellipsoid (Fig. 8) which is shown as a set of 2-D projections in Fig. 7A,B,C (e.g. Press et al., 1986). Each projection contains two ellipses. The smaller ellipse (dashed) denotes the 2-D, confidence region for two parameters where the 3rd is fixed at the optimal solution. For example, in Fig. 7A the dashed ellipse represents the intersection of the plane $A = 0.012 \mu\text{W m}^{-3}$ with the 3-D ellipsoid. It shows the range of values of q_m and T_m permitted (and the apparent correlation) at this value of A . The larger ellipse (solid line) is the shadow cast by the entire 3-D confidence envelope onto this two-dimensional plane. Axis parallel tangents to these “shadow” ellipses establish the maximum range of parameter values that are supported by the data at the 95% confidence limits. These values, however, are strongly correlated and cannot be combined arbitrarily.

The covariance between parameters at the solution (small ellipse) is not indicative of the overall covariance (large ellipse). For example, in Fig. 7B at a fixed value of q_m (15.1), the confidence envelope for A and T_m shows a weak positive correlation. Near the optimal solution at fixed q_m an increase in A (increased curvature) requires an increase in T_m . However, the correlation is actually strongly negative over the entire solution space (e.g. q_m is not fixed). An increase in A logically requires an increase in q_m and is best supported by lower T_m .

We have also modeled the effects of values of $B > 0$ corresponding to a 13 and 33% rise in K from the MOHO to the top of the asthenosphere (Fig. 7D,E,F; Table 2). Positive values of B mainly cause solutions to include lower values of A ; the optimal values of T_m and q_m change only slightly. Apparent variations in values of q_m mainly result from changes in the median values of K between simulations, rather than the value of B , because q_m scales directly to K (e.g. Jaupart et al., 1998). Increasing B also causes the solution region to enclose a larger range of negative

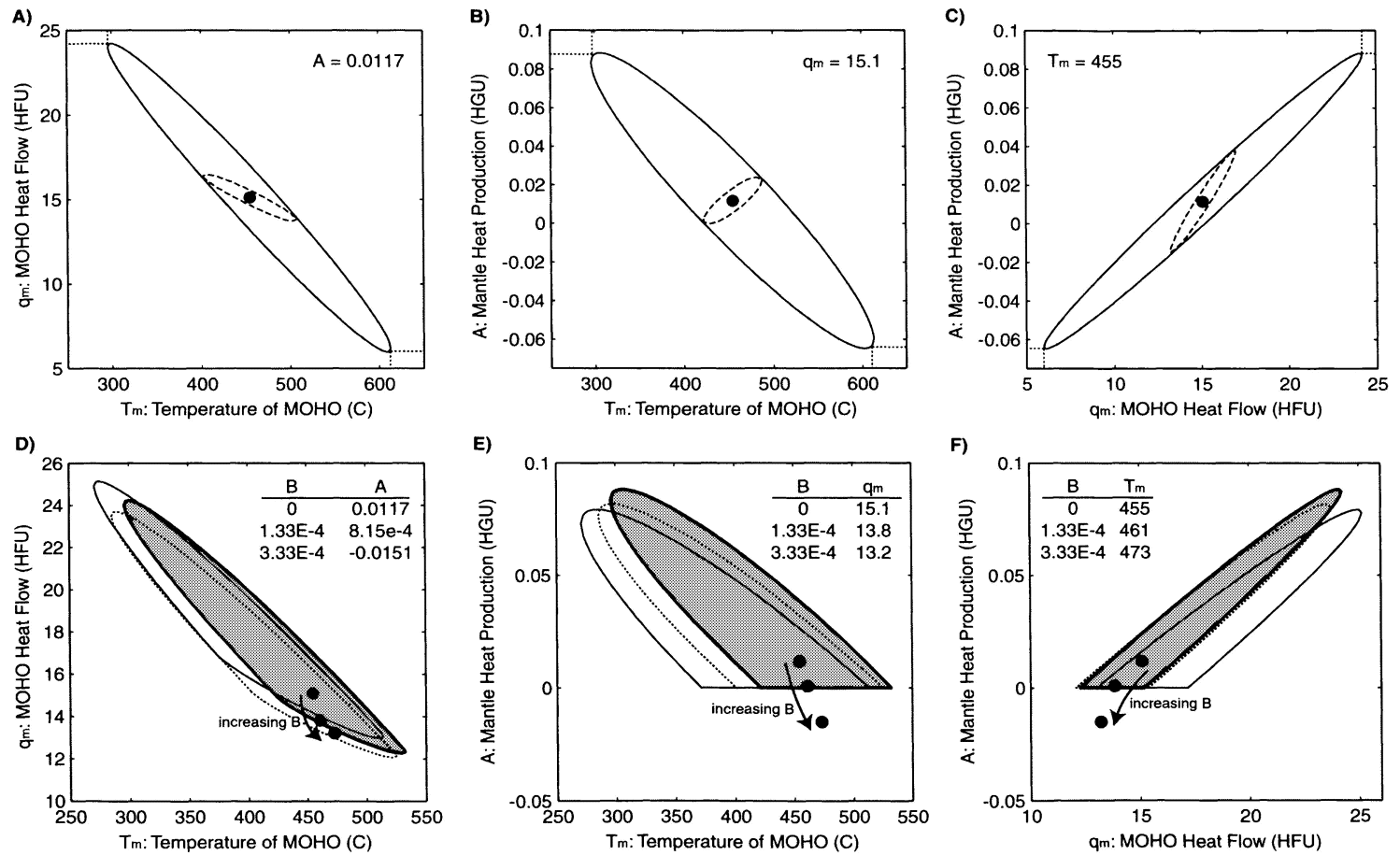


Fig. 7. Confidence ellipses (95%) to three parameter solutions plotted as (A) q_m vs. T_m , (B) A vs. T_m , and (C) A vs. q_m . Smaller ellipse denotes the 2-D, confidence region at the solution, the larger ellipse is the projection of the 3-D confidence ellipsoid onto the two-dimensional plane and shows the maximum range of parameter values permitted. The effects of changing B are shown in (D), (E), (F). Solutions are shown for B values of 0 K^{-1} (heavy line), $1.33E-4 \text{ K}^{-1}$ (dotted) and $3.33E-4 \text{ K}^{-1}$ (solid line); arrows denote effects of increasing B .

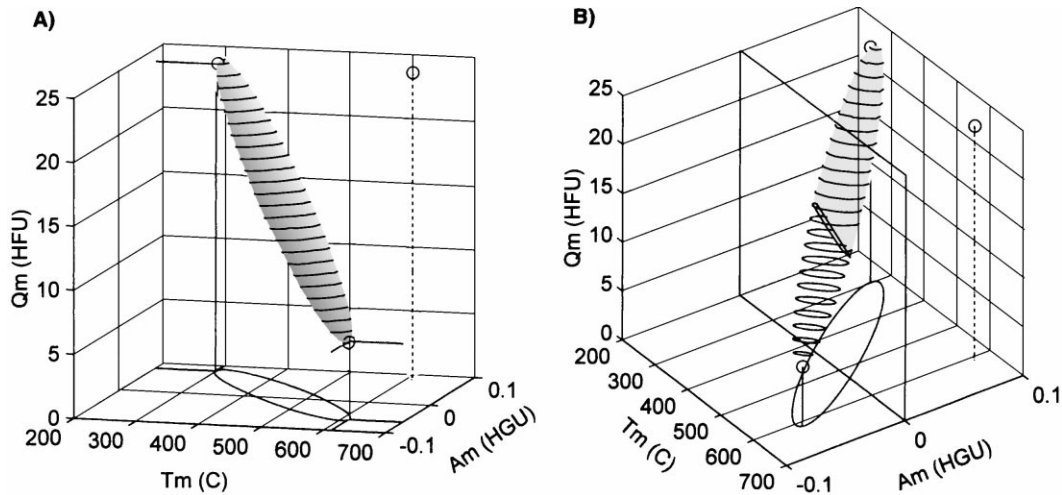


Fig. 8. Optimum solution to mantle geotherm problem shown as 3-D representation of the 95% confidence ellipsoid, (A) full solution space, (B) ellipsoid has been truncated to show only solutions with values of $A > 0$. Vertical dashed line denotes point that lies off ellipse but has parameters within “acceptable” range of values (see text).

values of A . In this case, the curvature of the geotherm is being attributed to combinations of $B > 0$ and $A < 0$. We have truncated the confidence ellipsoid to exclude the physically unrealistic solutions (e.g. $A < 0$) (Fig. 7D,E).

Fig. 8 shows a 3-D rendering of the ellipsoid that, at the 95% confidence level, encloses the full set of parameters that are consistent with the P – T data. The ellipsoid has two extreme end-points described by coordinates $[q_m$ – A – T_m]: $[24, 0.083, 296]$ and $[6.2, -0.060, 613]$ (Fig. 8A). These values are not equivalent to the 2σ bounding limits for each parameter shown in Fig. 7 (e.g. q_m : 5.98 to 24.2, A : -0.064 to 0.088, T_m : 612 to 296). Fig. 8A shows the nature of correlations between parameters and reinforces the idea that groups of parameters cannot be selected arbitrarily without the risk of “falling off the surface of the ellipsoid”. For example, although each of the values $q_m = 24$, $A = 0.083$ and $T_m = 612$ lies within the 95% confidence limits, the geotherm described by this combination of parameters lies well outside the 95% confidence limits of the solution. The solution region is further reduced by limiting the solutions to those with $A \geq 0$ (Fig. 8B).

A set of model geotherms represented by the ellipsoid surface (Fig. 8A,B) are generated and plotted

in Fig. 9. This set of geotherms (shading) represents the 95% confidence limits to the ideal geotherm given the original P – T data array. The P – T data are clearly well described by the 95% confidence limits on the geotherm. What is also immediately apparent from Figs. 8 and 9 is that, although the 3-D ellipse encompasses a wide range of values of q_m – A – T_m , the strong correlations between the model parameters generates a narrow family of geotherms.

The Slave mantle is best described by a reduced heat flow (q_m) of 15.1 mW m^{-2} and a MOHO temperature (T_m) of 455°C ; the corresponding best value for mantle heat production (A) is $0.012 \mu\text{W m}^{-3}$. The 95% confidence limits on the solution, in conjunction with the constraint that $A \geq 0$, restrict the values of reduced heat flow to 12.3 – 24.2 mW m^{-2} , the range of T_m to 534 to 296°C , and values of heat production to between 0 and $0.088 \mu\text{W m}^{-3}$. Our analysis of the solution space elucidates the strong correlation between model parameters and demonstrates that low values of T_m are correlated with high values of q_m and A and vice versa. For example, the maximum model value of T_m (534°C) can only be supported by zero heat production in the mantle and a low value of reduced heat flow (12.3 mW m^{-2}).

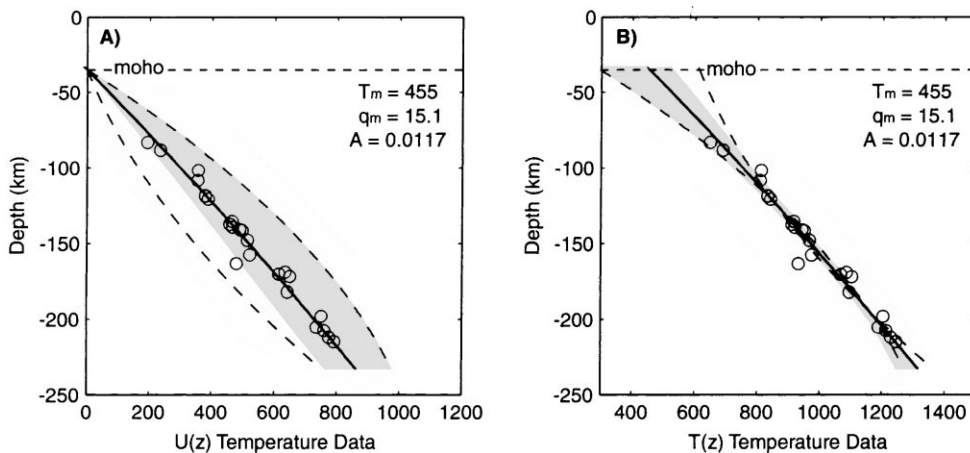


Fig. 9. Geotherms permitted by 95% confidence limits on q_m - T_m - A solution (Fig. 8) compared to the P - T array in (A) U - Z and (B) T - Z coordinate space. Shading denotes field of geotherms consistent with confidence limits and the restriction $A \geq 0$. Dashed lines denote the extreme solutions associated with the two ends of the ellipses; solid line is optimal solution.

7. Discussion

7.1. Comparative thermal properties of the Slave mantle

Our goal is to recover objective measures of the thermal state of the mantle from the petrology of mantle xenoliths. At the optimal value of A ($0.012 \mu\text{W m}^{-3}$) the ranges in q_m and T_m values are 14 – 16 mW m^{-2} and 400 – 500°C , respectively.

Temperatures at the MOHO (T_m) are constrained by measurements of compressional wave velocities at the MOHO. Specifically, Black and Braile (1982) argue that Pn velocities are negatively correlated with MOHO temperature. Pn velocities for the southern Slave vary between 8.05 and 8.15 km s^{-1} suggesting T_m values of 680 and 543°C , respectively (e.g. Hynman and Lewis, 1999). Further north on the Slave craton and closer to the Jericho kimberlite, the observed Pn velocities increase to values of 8.2 km s^{-1} (Mooney and Brocher, 1987) which corresponds to an equivalent MOHO temperature of 475°C .

We consider our optimal value (455°C) and our range of values (534 – 296°C) for T_m to be fully consistent with these geophysical observations, given that the uncertainties in the Pn- T_m relationship represent $\approx 150^\circ\text{C}$ (Black and Braile, 1982). We also expect values of T_m predicted from the Pn velocity to be

somewhat high because the constitutive relationship between Pn velocity and T_m is developed mainly for post-Archean mantle and assumes a uniform composition (Black and Braile, 1982). Younger, less depleted mantle lithosphere tends to be more enriched in Fe and olivine and thus, is seismically faster than older, depleted mantle underlying cratons. This implies that the Black and Braile (1982) model to cratonic mantle provides a maximum estimate for T_m .

Our modeling restricts values of reduced heat flow (q_m) between 12.3 and 24 mW m^{-2} . This range of values agrees broadly with other estimates of reduced and mantle heat flow for Precambrian terrains in general (e.g. Pinet and Jaupart, 1987; Jaupart et al., 1998; Rudnik et al., 1998). Specifically, our range of reduced heat flow, after correcting for mantle heat production, predicts a mantle heat flux of $13.3 \pm 2.5 \text{ mW m}^{-2}$ at depths below 150 km ; this value compares well with other estimates of mantle heat flux 10 – 15 mW m^{-2} (Pinet and Jaupart, 1987; Rudnik et al., 1998) and with the 12 mW m^{-2} mantle heat flux recently estimated for the Canadian shield (Jaupart et al., 1998; Jaupart and Mareschal, 1999).

7.2. Implications of A for eclogite abundance

Our results restrict mantle heat production in the Slave mantle lithosphere to values between

0 and 0.088 mW m^{-3} with an optimal value of $0.012 \text{ } \mu\text{W m}^{-3}$. These values of A can be used to constrain the proportions of eclogite within the Slave craton mantle.

The model estimates of A are substantially lower than the HP values calculated for Jericho xenoliths (Table 1, Appendix A) because Jericho xenoliths have been enriched in alkalis and incompatible elements such as Th and U by late mantle-derived metasomatic fluids (Russell and Kopylova, 1999). However, several eclogite samples (Appendix A) may be less affected by metasomatic fluids. They contain <3 vol.% late-stage, volatile-rich minerals indicative of mantle metasomatism (e.g. phlogopite) and they have lower calculated values of HP ($0.16\text{--}0.29 \text{ } \mu\text{W m}^{-3}$). Adopting the optimal value of A ($0.012 \text{ } \mu\text{W m}^{-3}$) and assuming an HP value of $0.01 \text{ } \mu\text{W m}^{-3}$ for mantle peridotite, this range of HP values for eclogite permit between 1.5 and 0.7 vol.% eclogite in the Slave mantle lithosphere.

These eclogite abundances are considerably less than the 3–15 vol.% estimated by Schulze (1989) for other cratonic mantle. However, Slave mantle eclogite abundances could be much higher (e.g. 20–10 vol.%) if we accept higher values of A (e.g. $0.04 \text{ } \mu\text{W m}^{-3}$) from within the 95% confidence limits (Fig. 7; Table 2) or if we consider peridotite to have lower HP (e.g. $<0.01 \text{ } \mu\text{W m}^{-3}$). Conversely, if we accept Schulze's (1989) values for eclogite abundance, then our model value of A ($0.012 \text{ } \mu\text{W m}^{-3}$) requires Slave mantle eclogite to have lower HP values (0.077 to $0.023 \text{ } \mu\text{W m}^{-3}$). At higher values of A (e.g. $0.08 \text{ } \mu\text{W m}^{-3}$), Schulze's (1989) proportions require eclogite to have HP values of $2.3\text{--}0.48 \text{ } \mu\text{W m}^{-3}$. These values overlap the HP values calculated for Jericho eclogite samples (Appendix A).

7.3. Implications of q_m for surface heat flow (q_o)

The model presented above has the attribute that we obtain estimates of mantle thermal properties without considering the structure and composition of the overlying crust. In this regard, we have improved on the work of Russell and Kopylova (1999) who inverted the same $P\text{--}T$ array data for crustal and mantle properties, including the depth of radiogenic heat

production in crustal rocks (D) and surface heat flow (q_o). They assumed a surface crustal HP (A_o) value of $2.16 \text{ } \mu\text{W m}^{-3}$, a value of $0.04 \text{ } \mu\text{W m}^{-3}$ for mantle HP and an exponential decrease in crustal HPE with depth. They estimated q_o and D to be 54.1 mW m^{-2} and 25.8 km , respectively, which corresponds well with direct measurements of surface heat flow and the crustal structure of the north-central Slave craton (cf. Russell and Kopylova, 1999). They also calculated values of reduced heat flow (e.g. 18.9 mW m^{-2}) that are higher than our optimal range of values ($14\text{--}16 \text{ mW m}^{-2}$) but predicted similar values of mantle heat flow (13.9 versus $13.3 \pm 2.5 \text{ mW m}^{-2}$).

Our model for the mantle geotherm has implications for surface heat flow in the Slave craton. Specifically, our estimate of reduced heat flow (q_m ; Table 2) can be used to predict q_o as a function of crustal properties. Lines of equal surface heat flow ($40, 50, 60 \text{ mW m}^{-2}$) have been drawn as a function of A_o and D (Fig. 10) for model values of q_m ($14\text{--}16 \text{ mW m}^{-2}$). The contours are drawn for two different distributions of HPE (Fig. 10A,B). Our estimates of q_m strongly support the Slave craton having a relatively high ($>50 \text{ mW m}^{-2}$) surface heat flow, given the observed crustal thickness (35 km) and high concentrations of HPE in surface crustal rocks ($>2 \text{ } \mu\text{W m}^{-3}$) (Bank et al., 2000; Russell and Kopylova, 1999).

8. Parameterization of lithospheric mantle

Our approach to constraining the thermal properties of the lithospheric mantle offers several advantages. Firstly, our method provides an objective estimate of the model parameters (q_m , A and T_m) that is based on petrological data and a small number of assumptions concerning the mantle. Specifically, our model is decoupled from any decisions about the thermal properties of the crust (e.g. crustal heat production). The only linkage between our model mantle geotherm and crustal heat flow is the parameter q_m , which is the reduced heat flow entering the crust. We argue that this estimate of q_m is less biased than are values that derive from measurements of surface heat flow or from models that incorporate crustal thermal parameters. Our mantle heat flow estimate, also, is a product only of mantle heat production and primary mantle heat flow. On this basis, we argue that our results provide a more

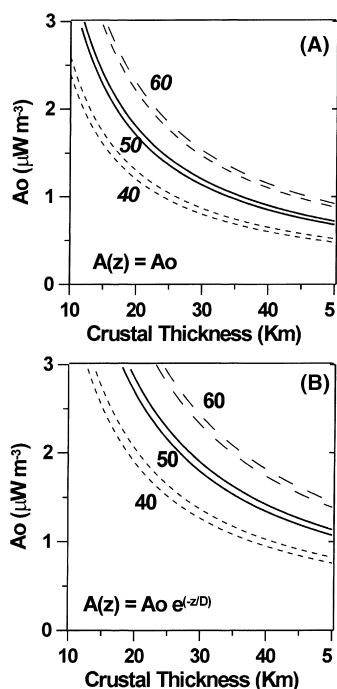


Fig. 10. Implications of the model mantle geotherm for surface heat flow. A range of reduced heat flow values ($q_m = 14\text{--}16\text{ mW m}^{-2}$) is used to draw contours of surface heat flow (40, 50, 60 mW m^{-2}) as a function of thickness of the heat producing crustal layer and radiogenic heat production of surface crustal rocks (A_o). Distribution of heat producing elements in the crust is assumed to be: (A) constant, or (B) decreasing exponentially with depth.

objective characterization of the Slave mantle lithosphere than do results derived from models that couple crustal thermal properties to the mantle thermal regime (e.g. Russell and Kopylova, 1999; MacKenzie and Canil, 1999).

Solving for the steady-state geotherm as an overdetermined system of equations Eq. (9) also facilitates a statistical analysis of the model parameters. For example the magnitude and nature of correlations between fit parameters can be clearly illustrated. Furthermore, because the problem is generally linear in the fit parameters, we are able explicitly to calculate the statistical uncertainties on the model parameters. These estimates are critical in our quest to constrain the maximum and minimum bounds on lithospheric mantle heat production and the temperature dependence of K .

We have shown that the mantle P – T array is permissive of a large range of model parameters: reduced heat flow (q_m), MOHO temperatures (T_m) and mantle heat production (A). However, these properties are strongly correlated. Therefore, even though we are obliged to consider a wide range of model mantle properties, the strong correlations between parameters create a very narrow band of model geotherms that are consistent with the data at the 95% confidence limit. This point cannot be emphasized enough; values of model parameters cannot be combined arbitrarily to generate valid geotherms.

This analysis has implications for our attempts to characterize the thermal structure of cratonic mantle lithosphere. Our conclusion is that description of the mantle lithosphere with a single parameter is highly misleading and cannot possibly lead to a unique or meaningful description of the thermal regime of the mantle. Rather, differences between the thermal states of different mantle lithospheres can only be recognized by considering several thermal properties simultaneously. We suggest that mantle lithosphere can be uniquely described by three parameters: q_m – A – T_m if the covariances between these properties are also considered. These parameters represent specific mantle properties and they are fundamental to the mathematical description of the P – T array (e.g. mantle geotherm). Essentially they represent the intercept value (T_m) of the P – T array at that point (q_m) and the curvature (A) of the array.

Acknowledgements

This research was funded by NSERC through the Research Grants Program. Our work benefitted from fruitful discussions with C. Bank. Insightful criticisms garnered from anonymous reviewers provided a basis for improving the clarity of our arguments. RIGD is a consortium of university researchers collaborating on problems in dynamic geochemical systems.

Appendix A. Major and trace element compositions of eclogite xenoliths from Jericho kimberlite pipe and values of heat production

Label	20-7	16-4	55-4	F6n-Ec13	52-5	47-2	42-3	47-8	21-8	06-11 ^a	D.L.
SiO ₂	43.69	43.6	42.83	46.34	47.41	41.02	41.21	44.45	43.64	45.74	
TiO ₂	0.241	0.287	0.885	1.151	0.34	0.46	2.802	1.994	0.342	1.678	
Al ₂ O ₃	15.84	12.16	15.11	10.35	12.6	14.26	12.1	12.67	13.78	9.43	
FeO	9.35	6.23	6.69	5.34	5.44	7.59	8.13	8.87	5.28	7.37	
Fe ₂ O ₃	3.53	4.13	3.29	4.23	1.46	4.51	6.48	3.75	2.14	5.65	
MnO	0.22	0.19	0.20	0.14	0.13	0.19	0.22	0.19	0.29	0.23	
MgO	13.84	19.68	14.73	15.12	16.95	16.07	11.75	11.58	19.4	14.61	
CaO	9.79	9.02	10.6	11.29	10.56	8.86	11.82	10.73	10.09	11.56	
Na ₂ O	1.35	0.65	1.95	2.61	2.09	1.54	1.68	2.3	0.69	1.02	
K ₂ O	0.37	0.34	0.2	0.07	0.65	0.37	0.28	0.79	1.36	0.75	
P ₂ O ₅	0.04	0.04	0.04	0.03	0.06	0.05	0.24	0.10	0.07	0.04	
LOI	1.41	3.31	3.2	3.09	2.02	4.78	2.88	2.25	2.32	1.4	
Total	99.64	99.63	99.73	99.76	99.7	99.7	99.6	99.68	99.41	99.48	
Fe ₂ O ₃ (T)	13.92	11.06	10.73	10.16	7.51	12.95	15.52	13.61	8.01	13.84	
K ₂ O	0.34	0.29	0.2	0.07	0.58	0.28	0.22	0.8	1.43	0.64–0.74	0.01
K (%)	0.28	0.24	0.17	0.06	0.48	0.23	0.18	0.66	1.19	0.53–0.61	0.01
K (ppm)	2823	2407	1660	581	4815	2324	1826	6641	11871	5312–6143	83
Th (ppm)	2	2.6	1.3	1.6	5.5	2	2.3	2.2	5.4	2.5–2.9	0.1
U (ppm)	0.3	0.7	0.1	5	0.5	0.4	0.4	0.7	0.5	0.3–0.4	0.1
mW m ⁻³	0.2947	0.4644	0.1602	1.6879	0.6761	0.3199	0.3396	0.479	0.7485	0.365–0.44	0.04

^a Concentrations of heat producing elements were measured twice.

References

- Bailey, D.K., 1980. Volatile flux, geotherms, and the generation of the kimberlite-carbonatite-alkaline magma spectrum. *Mineral. Mag.* 43, 695–699.
- Bank, C.-G., Bostock, M.G., Ellis, R.M., Cassidy, J.F., 2000. A reconnaissance teleseismic study of the upper mantle and transition zone beneath the Archean Slave craton in NW Canada. *Tectonophysics* 319, 151–166.
- Bostock, M.G., 1998. Mantle stratigraphy and evolution of the Slave province. *J. Geophys. Res.* 103, 21183–21200.
- Black, P.R., Braile, L.W., 1982. Pn velocity and cooling of the continental lithosphere. *J. Geophys. Res.* 87 (B13), 10557–10568.
- Boyd, F.R., 1987. High- and low-temperature garnet peridotite xenoliths and their possible relation to the lithosphere-asthenosphere boundary beneath southern Africa. In: Nixon, P.H. (Ed.), *Mantle Xenoliths*. Wiley, New York, pp. 403–412.
- Boyd, F.R., Pokhilenko, N.P., Pearson, D.G., Mertzman, S.A., Sobolev, N.V., Finger, L.W., 1997. Composition of the Siberian cratonic mantle: evidence from Udachnaya peridotite xenoliths. *Contrib. Miner. Petrol.* 128, 228–246.
- Brey, G.P., Kohler, T., 1990. Geothermobarometry in four-phase lherzolites. II. New thermobarometers and practical assessment of existing thermobarometers. *J. Petrol.* 31, 1353–1378.
- Carmichael, R.S., 1984. *CRC Handbook of Physical Properties of Rocks*, Vol. III. CRC Press, FL.
- Cermak, V., Huckenholz, H.G., Rybach, L., Schmid, R., Schopper, J.R., Schuch, M., Stoffer, D., Wohlenberg, J., 1982. In: Angenheister, G. (Ed.), *Physical Properties of Rocks*, Vol. 1a. Springer, Heidelberg.
- Cook, F.A., Van der Velden, A.J., Hall, K.W., Roberts, B.R., 1997. LITHOPROBE SNORCLE-ing beneath the northwestern Canadian shield: deep lithospheric reflection profiles from the Cordillera to the Archean Slave province. In: Cook, F., Erdmer, P. (Eds.), *SNORCLE Transect and Cordilleran Tectonics Workshop Meeting*, Lithoprobe Report No. 56 58–62, 1997.
- Cookenboo, H., 1998. Emplacement history of the Jericho kimberlite pipe, northern Canada. In: *Proceedings of Extended Abstracts of the 17th International Kimberlite Conference*, pp. 161–163.
- Ellis, D.J., Green, D.H., 1979. An experimental study of the effect of Ca upon garnet-clinopyroxene Fe-Mg exchange equilibria. *Contrib. Mineral. Petrol.* 71, 13–33.
- Ganguly, J., Singh, R.N., Ramana, D.N., 1995. Thermal perturbation during charnokitization and granulite facies metamorphism in southern India. *J. Metam. Geol.* 13, 419–430.
- Griffin, W.L., Doyle, B.J., Ryan, C.G., Pearson, N.J., O'Reilly, S.Y., Davies, R., Kivi, K., van Achterbergh, E., Natapov, L.M., 1999. Layered mantle lithosphere in the Lac de Gras Area, Slave craton: composition, structure and origin. *J. Petrol.* 40, 705–727.
- Grutter, H.S., Apter, D.B., Kong, J., 1999. Crust-Mantle Coupling: Evidence from mantle-derived xenocrystic garnets. In: Gurney, J.J., Richardson, S.R. (Eds.), *Proceedings of 7th International Kimberlite Conference*, Red Roof Designs, Cape Town, pp. 307–312.

- Harte, B., Hawkesworth, C.J., 1989. Mantle domains and mantle xenoliths. In: Ross, J., Jaques, A.L., Ferguson, J., Green, D.H., O'Reilly, S.Y., Danchin, R.V., Janse, A.J. (Eds.), *Kimberlites and Related Rocks*, Geol. Soc. Aust. (special publication) No. 14, Blackwell Scientific Publications, Victoria, pp. 649–686.
- Helmstaedt, H., Schulze, D.J., 1989. Southern African kimberlites and their mantle sample: implications for Archean tectonics and lithosphere evolution. In: Ross, J. (Ed.), *Kimberlites and Related Rocks*, Vol. 1, Geol. Soc. Aust. (special publication 14), pp. 358–368.
- Hyndman, R.D., Lewis, T.J., 1999. Geophysical consequences of the Cordillera-craton thermal transition in southwestern Canada. *Tectonophysics* 306, 397–422.
- Jaupart, C., Mareschal, J.C., Guillou-Frottier, L., Davaille, A., 1998. Heat flow and thickness of the lithosphere in the Canadian shield. *J. Geophys. Res.* 103, 15269–15286.
- Jaupart, C., Mareschal, J.C., 1999. The thermal structure and thickness of continental roots. *Lithos* 48, 93–114.
- Jones, A.G., Ferguson, I., Evans, R., Chave, A., 2000. The electric Slave craton. In: Cook, F., Erdmer, P. (Eds.), *SNORCLE Transect and Cordilleran Tectonics Workshop Meeting*, February 25–27, University of Calgary, Lithoprobe Report No 72, pp. 36–42.
- Katsura, T., 1995. Thermal diffusivity of olivine under upper mantle conditions. *Geophys. J. Int.* 122, 63–69.
- Kopylova, M.G., Russell, J.K., 2000. Chemical stratification of cratonic lithosphere: constraints from the northern Slave craton. *Earth Planet. Sci. Lett.* 181, 71–87.
- Kopylova, M.G., Russell, J.K., Cookenboo, H., 1999a. Petrology of peridotite and pyroxenite xenoliths from the Jericho kimberlite: implications for thermal state of the mantle beneath the Slave craton, northern Canada. *J. Petrol.* 40, 79–104.
- Kopylova, M.G., Russell, J.K., Cookenboo, H., 1999b. Mapping the lithosphere beneath the north-central Slave craton, In: Gurney, J.J., Richardson, S. (Eds.), *Proceedings of the 7th International Kimberlite Conference*, Red Roof Design, Cape Town, pp. 468–479.
- Lee, C.-T., Rudnick, R.L., 2000. Compositionally stratified cratonic lithosphere: petrology and geochemistry of peridotite xenoliths from the Labait tuff cone, Tanzania. In: J.J. Gurney, J.J., Richardson, S.R. (Eds.), *Proceedings of the 7th International Kimberlite Conference*, Red Roof Designs, Cape Town, pp. 503–521.
- MacKenzie, J.M., Canil, D., 1999. Composition and thermal evolution of cratonic mantle beneath the central Archean Slave province, NWT, Canada. *Contrib. Miner. Petrol.* 134, 313–324.
- Mooney, W.D., Brocher, T.M., 1987. Coincident seismic reflection/refraction studies of the continental lithosphere. *Rev. Geophys.* 25, 723–742.
- Nixon, P.H., Rogers, N.W., Gibson, I.L., Grey, A., 1981. Depleted and fertile mantle xenoliths from southern African kimberlites. *Ann. Rev. Earth Planet. Sci.* 9, 285–309.
- Nyblade, A.A., Pollack, H.N., 1993. A global analysis of heat flow from precambrian terrains: implications for the thermal structure of Archean and proterozoic lithosphere. *J. Geophys. Res.* 98, 12207–12218.
- O'Reilly, S.Y., Griffin, W.L., 1996. 4-D lithosphere mapping: methodology and examples. *Tectonophysics* 262, 3–18.
- Ozisik, M.N., 1993. *Heat Conduction*, 2nd Edition. Wiley, New York.
- Padgham, W.A., Fyson, W.K., 1992. The Slave province: a distinct craton. *Can. J. Earth Sci.* 29, 2072–2086.
- Pearson, N.J., Griffin, W.L., Doyle, B.J., O'Reilly, S.Y., van Achtenbergh, E., Kivi, K., 1999. Xenoliths from kimberlite pipes of the Lac de Gras Area, Slave craton, Canada. In: Gurney, J.J., Richardson, S.R. (Eds.), *Proceedings of the 7th International Kimberlite Conference*, Red Roof Designs, Cape Town, pp. 644–658.
- Pinet, C., Jaupart, C., 1987. The vertical distribution of radiogenic heat production in the precambrian crust of Norway and Sweden: geothermal implications. *Geophys. Res. Lett.* 14, 260–263.
- Pollack, H.N., Chapman, D.S., 1977. On the regional variation of heat flow, geotherms and lithospheric thickness. *Tectonophysics* 38, 279–296.
- Press, W.H., Flannery, B.P., Teukolsky, S.A., Vetterling, W.T., 1986. *Numerical Recipes: The Art of Scientific Computing*, Cambridge University Press, Cambridge.
- Price, S.E., Russell, J.K., Kopylova, M.G., 2000. Primitive magma from the Jericho pipe, NWT, Canada: constraints on primary kimberlite melt chemistry. *J. Petrol.* 41, 789–808.
- Rudnik, R.L., McDonough, W.F., O'Connell, R.J., 1998. Thermal structure, thickness and composition of continental lithosphere. *Chem. Geol.* 145, 399–415.
- Russell, J.K., Kopylova, M.G., 1999. A steady-state conductive geotherm for the north-central Slave, Canada: Inversion of petrological data from the Jericho kimberlite pipe. *J. Geophys. Res.* 104, 7089–7101.
- Schatz, H.F., Simmons, G., 1972. Thermal conductivity of Earth minerals at high temperatures. *Geophys. Res.* 77, 6966–6983.
- Schulze, D.J., 1989. Constraints on the abundance of eclogite in the upper mantle. *J. Geophys. Res.* 94, 4205–4212.